nerve atrophy, severe psychosis, depressive state, chorea-athetosis, spasticity, and unresponsive to levodopa(Gregory, et al., 2009). PKAN has some common features such as oculomotor abnormalities, pyramidal sign, or the eye-of-the-tiger sign on brain MRI, features that are less common in BPAN. Brain MRI imaging of PKAN and BPAN share some common features such as iron accumulation of globus pallidus, subthalamus, and nigra(Schneider, et al., 2013). The second type of NBIA is *PLA2G6* associated neurodegenration, which is commonly characterized as dystonia-parkinsonism combined with pyramidal signs, eye movement abnormalities, cognitive declines and psychiatric features. With the exception of cognitive decline, these symptoms are less prevalent in BPAN. In addition, neuroimaging of *PLA2G6* associated neurodegenration patients indicates that iron accumulation is not a major feature. mitochondrial protein-associated neurodegeneration has the symptoms of spastic paraparesis, neuropathy, optic atrophy, and psychiatric symptoms, which are not generally seen in BPAN.

All of the identified mutations in *WDR45* were located within exons 5-10 and RT-PCR showed a heterozygous mutation in cDNA in two patients, supporting a previous case report (Saitsu, et al., 2013). Some of the cases with BPAN showed biallelic expression, even on the X chromosome and thus did not obey X-inactivation. In female mammals, about 15% of X-linked genes escape inactivation (Carrel and Willard, 2005). Thus, among our female patients, the co-existence of wild type and mutant alleles was admitted in *WDR45* cDNA. *WDR45* encodes WIPI4, a seven-bladed beta-propeller protein involved in autophagy and part of the group of WD40 repeat proteins which are involved in cell cycle control, apoptosis, and autophagy (Behrends, et al., 2010). WIPI4 regulates distribution of Atg9A-marked vesicles to autophagosomes that complete the autophagosome maturation (Itakura, et al., 2012,Orsi, et al., 2012). Mutations in *WDR45* may result in impaired autophagy and lead to the accumulation of abnormal proteins. *WDR45* may be involved in mechanisms that result in accumulation of iron in the brain and subsequently disturb brain development.

One of the fascinating features of NBIA cases is iron accumulation in the globus pallidus, the substantia nigra, or cerebral peduncles. It was reported that iron homeostasis, mitochondrial ferritin, and neurological disorders have strong association via the molecular pathways of transferrin, ferritin, mitoferrin, and ceruloplasmin(Schneider, et al., 2013). The dysregulation of mitochondrial iron and ferritin especially in the outer cellular membrane has been reported to result in excess production of reactive oxygen species (Eaton and Qian, 2002). Oxidative stress causes neuronal death and denatured mitochondria in the substantia nigra, not only in the hereditary form of PD but also

sporadic PD cases (Henchcliffe and Beal, 2008,Jenner, 2003). *WDR45* mutations may relate to iron metabolism, mitochondrial denature, destruction of membranes or emerging dystrophic axonal spheroids, directly or indirectly, via the common pathway of NBIA and PD.

5. Conclusions

We found seven patients diagnosed with BPAN harboring *WDR45* mutations, suggesting *WDR45* as the most prevalent cause of BPAN in our Japanese population. These patients share a common clinical phenotypes with prominent features similar to those seen in previous cases. Importantly, levodopa presents good response for motor symptoms. These results contribute to further understanding of BPAN and NBIA types and can help in the diagnosis of BPAN.

Acknowledgement

We obtained insightful comments from Dr. Carles Vilariño-Güell at the University of British Columbia, Vancouver, Canada. KN was supported by JSPS KAKNEHI Grant Number 2586076. We are grateful for the Grant-in-Aid for Scientific Research on Innovative Areas (MF, SS, and NH), the Grant-in-Aid for Young Scientists (YL, SS and KN), the Grant-in-Aid for Challenging Exploratory Research (SS), Grant-in-Aid for Scientific Research (MF and NH) from Japan Society for the Promotion of Science, Grant-in-Aid for Scientific Research on Priority Areas (SS and NH) from the Japanese Ministry of Education, Culture, Sports, Science and Technology, and the Grants-in-Aid from the Research Committee of CNS Degenerative Diseases (NH), the Grant-in-Aid for Health Labour Sciences Research Grant (NH) from Ministry of Health Labour and Welfare, and grants from the Life Science Foundation, the Takeda Scientific Foundation, the Cell Science Research Foundation, and the Nakajima Foundation (SS).

References

Behrends, C., Sowa, M.E., Gygi, S.P., Harper, J.W. 2010. Network organization of the human autophagy system. Nature 466(7302), 68-76. doi:nature09204 [pii]

10.1038/nature09204.

Carrel, L., Willard, H.F. 2005. X-inactivation profile reveals extensive variability in X-linked gene expression in females. Nature 434(7031), 400-4. doi:nature03479 [pii]

10.1038/nature03479.

Dusi, S., Valletta, L., Haack, T.B., Tsuchiya, Y., Venco, P., Pasqualato, S., Goffrini, P., Tigano, M., Demchenko, N., Wieland, T., Schwarzmayr, T., Strom, T.M., Invernizzi, F., Garavaglia, B., Gregory, A., Sanford, L., Hamada, J., Bettencourt, C., Houlden, H., Chiapparini, L., Zorzi, G., Kurian, M.A., Nardocci, N., Prokisch, H., Hayflick, S., Gout, I., Tiranti, V. 2014. Exome sequence reveals mutations in CoA synthase as a cause of neurodegeneration with brain iron accumulation. Am J Hum Genet 94(1), 11-22. doi:S0002-9297(13)00523-5 [pii]

10.1016/j.ajhg.2013.11.008.

Eaton, J.W., Qian, M. 2002. Molecular bases of cellular iron toxicity. Free Radic Biol Med 32(9), 833-40. doi:S0891584902007724 [pii].

Gregory, A., Polster, B.J., Hayflick, S.J. 2009. Clinical and genetic delineation of neurodegeneration with brain iron accumulation. J Med Genet 46(2), 73-80. doi:jmg.2008.061929 [pii]

10.1136/jmg.2008.061929.

Haack, T.B., Hogarth, P., Kruer, M.C., Gregory, A., Wieland, T., Schwarzmayr, T., Graf, E., Sanford, L., Meyer, E., Kara, E., Cuno, S.M., Harik, S.I., Dandu, V.H., Nardocci, N., Zorzi, G., Dunaway, T., Tarnopolsky, M., Skinner, S., Frucht, S., Hanspal, E., Schrander-Stumpel, C., Heron, D., Mignot, C., Garavaglia, B., Bhatia, K., Hardy, J., Strom, T.M., Boddaert, N., Houlden, H.H., Kurian, M.A., Meitinger, T., Prokisch, H., Hayflick, S.J. 2012. Exome sequencing reveals de novo WDR45 mutations causing a phenotypically distinct, X-linked dominant form of NBIA. Am J Hum Genet 91(6), 1144-9. doi:S0002-9297(12)00578-2 [pii]

10.1016/j.ajhg.2012.10.019.

Hartig, M.B., Iuso, A., Haack, T., Kmiec, T., Jurkiewicz, E., Heim, K., Roeber, S., Tarabin, V., Dusi, S., Krajewska-Walasek, M., Jozwiak, S., Hempel, M., Winkelmann, J., Elstner, M., Oexle, K., Klopstock, T., Mueller-Felber, W., Gasser, T., Trenkwalder, C., Tiranti, V., Kretzschmar, H., Schmitz, G., Strom, T.M., Meitinger, T., Prokisch, H. 2011. Absence of an orphan mitochondrial protein, c19orf12, causes a distinct clinical subtype of neurodegeneration with brain iron accumulation. Am J Hum Genet 89(4), 543-50. doi:S0002-9297(11)00397-1 [pii]

10.1016/j.ajhg.2011.09.007.

Hayflick, S.J., Kruer, M.C., Gregory, A., Haack, T.B., Kurian, M.A., Houlden, H.H., Anderson, J., Boddaert, N., Sanford, L., Harik, S.I., Dandu, V.H., Nardocci, N., Zorzi, G., Dunaway, T., Tarnopolsky, M., Skinner, S., Holden, K.R., Frucht, S., Hanspal, E., Schrander-Stumpel, C., Mignot, C., Heron, D., Saunders, D.E., Kaminska, M., Lin, J.P., Lascelles, K., Cuno, S.M., Meyer, E., Garavaglia, B., Bhatia, K., de Silva, R., Crisp, S., Lunt, P., Carey, M., Hardy, J., Meitinger, T., Prokisch, H., Hogarth, P. 2013. beta-Propeller protein-associated neurodegeneration: a new X-linked dominant disorder with brain iron accumulation. Brain 136(Pt 6), 1708-17. doi:awt095 [pii]

10.1093/brain/awt095.

Henchcliffe, C., Beal, M.F. 2008. Mitochondrial biology and oxidative stress in Parkinson disease pathogenesis. Nat Clin Pract Neurol 4(11), 600-9. doi:ncpneuro0924 [pii]

10.1038/ncpneuro0924.

Hogarth, P., Gregory, A., Kruer, M.C., Sanford, L., Wagoner, W., Natowicz, M.R., Egel, R.T., Subramony, S.H., Goldman, J.G., Berry-Kravis, E., Foulds, N.C., Hammans, S.R., Desguerre, I., Rodriguez, D., Wilson, C., Diedrich, A., Green, S., Tran, H., Reese, L., Woltjer, R.L., Hayflick, S.J. 2013. New NBIA subtype: genetic, clinical, pathologic, and radiographic features of MPAN. Neurology 80(3), 268-75. doi:WNL.0b013e31827e07be [pii]

10.1212/WNL.0b013e31827e07be.

Ichinose, Y., Miwa, M., Onohara, A., Obi, K., Shindo, K., Saitsu, H., Matsumoto, N., Takiyama, Y. 2014. Characteristic MRI findings in beta-propeller protein-associated neurodegeneration (BPAN). Neurol Clin Pract 4(2), 175-7. doi:10.1212/01.CPJ.0000437694.17888.9b

NEURCLINPRACT2013003822 [pii].

Itakura, E., Kishi-Itakura, C., Koyama-Honda, I., Mizushima, N. 2012. Structures containing Atg9A and the ULK1 complex independently target depolarized mitochondria at initial stages of Parkin-mediated mitophagy. J Cell Sci 125(Pt 6), 1488-99. doi:jcs.094110 [pii]

10.1242/jcs.094110.

Jenner, P. 2003. Oxidative stress in Parkinson's disease. Ann Neurol 53 Suppl 3, S26-36; discussion S-8. doi:10.1002/ana.10483.

Orsi, A., Razi, M., Dooley, H.C., Robinson, D., Weston, A.E., Collinson, L.M., Tooze, S.A. 2012. Dynamic and transient interactions of Atg9 with autophagosomes, but not membrane integration, are required for autophagy. Mol Biol Cell 23(10), 1860-73. doi:mbc.E11-09-0746 [pii]

10.1091/mbc.E11-09-0746.

Paisan-Ruiz, C., Bhatia, K.P., Li, A., Hernandez, D., Davis, M., Wood, N.W., Hardy, J., Houlden, H., Singleton, A., Schneider, S.A. 2009. Characterization of PLA2G6 as a locus for dystonia-parkinsonism. Ann Neurol 65(1), 19-23. doi:10.1002/ana.21415.

Rathore, G.S., Schaaf, C.P., Stocco, A.J. 2014. Novel mutation of the WDR45 gene causing beta-propeller protein-associated neurodegeneration. Mov Disord 29(4), 574-5. doi:10.1002/mds.25868.

Saitsu, H., Nishimura, T., Muramatsu, K., Kodera, H., Kumada, S., Sugai, K., Kasai-Yoshida, E., Sawaura, N., Nishida, H., Hoshino, A., Ryujin, F., Yoshioka, S., Nishiyama, K., Kondo, Y., Tsurusaki, Y., Nakashima, M., Miyake, N., Arakawa, H., Kato, M., Mizushima, N., Matsumoto, N. 2013. De novo mutations in the autophagy gene WDR45 cause static encephalopathy of childhood with neurodegeneration in adulthood. Nat Genet 45(4), 445-9, 9e1. doi:ng.2562 [pii]

10.1038/ng.2562.

Schneider, S.A., Dusek, P., Hardy, J., Westenberger, A., Jankovic, J., Bhatia, K.P. 2013. Genetics and Pathophysiology of Neurodegeneration with Brain Iron Accumulation (NBIA). Curr Neuropharmacol 11(1), 59-79. doi:10.2174/157015913804999469

CN-11-59 [pii].

Stirnimann, C.U., Petsalaki, E., Russell, R.B., Muller, C.W. 2010. WD40 proteins propel cellular networks. Trends Biochem Sci 35(10), 565-74. doi:S0968-0004(10)00072-1 [pii]

10.1016/j.tibs.2010.04.003.

Verhoeven, W.M., Egger, J.I., Koolen, D.A., Yntema, H., Olgiati, S., Breedveld, G.J., Bonifati, V., van de Warrenburg, B.P. 2014. Beta-propeller protein-associated neurodegeneration (BPAN), a rare form of NBIA: Novel mutations and neuropsychiatric phenotype in three adult patients. Parkinsonism Relat Disord 20(3), 332-6. doi:S1353-8020(13)00419-7 [pii]
10.1016/j.parkreldis.2013.11.019.

Wilson, G.R., Sim, J.C., McLean, C., Giannandrea, M., Galea, C.A., Riseley, J.R., Stephenson, S.E., Fitzpatrick, E., Haas, S.A., Pope, K., Hogan, K.J., Gregg, R.G., Bromhead, C.J., Wargowski, D.S., Lawrence, C.H., James, P.A., Churchyard, A., Gao, Y., Phelan, D.G., Gillies, G., Salce, N., Stanford, L., Marsh, A.P., Mignogna, M.L., Hayflick, S.J., Leventer, R.J., Delatycki, M.B., Mellick, G.D., Kalscheuer, V.M., D'Adamo, P., Bahlo, M., Amor, D.J., Lockhart, P.J. 2014. Mutations in RAB39B Cause X-Linked Intellectual Disability and Early-Onset Parkinson Disease with alpha-Synuclein Pathology. Am J Hum Genet 95(6), 729-35. doi:S0002-9297(14)00463-7 [pii]
10.1016/j.ajhg.2014.10.015.

Figure legends

Figure 1: Direct sequencing of *WDR45* shows mutant sequence (top) and wild-type sequence (bottom) of seven patients. Heterozygous mutations were observed in all cases.

Figure 2: The results of RT-PCR indicate homozygous mutations of cDNA in Case 1 and 7, and heterozygous mutations in Case 2 and 6.

Figure 3: Brain MRI imaging of axial view indicates prominent features in patients with *WDR45* mutations, (a) the halo in the substantia nigra in axial T1WI; (b) hypointense in T2WI in cerebral peduncles; and (c) marked atrophy in bilateral fronto-temporal lobe in T1WI of case 2. (d) in T1WI and (e) in T2WI of Case 3 are similar to findings of (a) and (b). (f) and (g) of Case 3 show hypointense signal in T1WI and T2 WI in bilateral globus pallidus, and disproportional atrophy in left temporal lobe. (h), (i), and (j) of Case 4 demonstrate similar findings to (a), (b) and (g), especially marked disproportional atrophy in left temporal lobe. (k) of Case 5 indicate the diffuse atrophy in frontal-temporal lobes in axial T1. (l) of Case 5 is the same as findings in (b). (m), (n), (o) of Case 7 are similar to findings in (a), (b), and (g). As normal control, (p) mid brain in T1WI, (q) in T2WI, and (r) globus pallidus and basal ganglia in T1WI, (s) in T2WI; female and 33 years old.

Table 1: Clinical overview of the assessed patients and the results of gene screening related with NBIA.

Table 2: Clinical overview of the seven patients with *WDR45* gene mutations.

NA; not assessed.

Table 3: Summary of clinical data combined with the previous reports and our cases.

Neurobiology of Aging 35 (2014) 2656.e17–2656.e23

Contents lists available at ScienceDirect

Neurobiology of Aging

journal homepage: www.elsevier.com/locate/neuaging

Identification of a Japanese family with *LRRK2* p.R1441G-related Parkinson's disease

Taku Hatano [a,*], Manabu Funayama [a,b], Shin-ichiro Kubo [a], Ignacio F. Mata [d,e], Yutaka Oji [a], Akio Mori [a], Cyrus P. Zabetian [d,e], Sarah M. Waldherr [d,e], Hiroyo Yoshino [b], Genko Oyama [a], Yasushi Shimo [a,c], Ken-ichi Fujimoto [f], Hirokazu Oshima [g], Yasuto Kunii [g], Hirooki Yabe [g], Yoshikuni Mizuno [a], Nobutaka Hattori [a,b,*]

[a] *Department of Neurology, Juntendo University School of Medicine, Tokyo, Japan*
[b] *Research Institute for Diseases of Old Age, Juntendo University Graduate School of Medicine, Tokyo, Japan*
[c] *Department of Research and Therapeutics for Movement Disorders, Juntendo University School of Medicine, Tokyo, Japan*
[d] *Geriatric Research Education and Clinical Center, VA Puget Sound Health Care System, Seattle, WA, USA*
[e] *Department of Neurology, University of Washington, Seattle, WA, USA*
[f] *Jichi-idai Station Brain Clinic, Tochigi, Japan*
[g] *Department of Neuropsychiatry, Fukushima Medical University, Fukushima, Japan*

ARTICLE INFO

Article history:
Received 15 February 2014
Received in revised form 26 May 2014
Accepted 27 May 2014
Available online 2 June 2014

Keywords:
Parkinson's disease
LRRK2
p.R1441G
Asia
Intrafamilial clinical heterogeneity

ABSTRACT

Leucine-rich repeat kinase 2 (*LRRK2*) is a causative gene of autosomal dominant familial Parkinson's disease (PD). We screened for *LRRK2* mutations in 3 frequently reported exons (31, 41, and 48) in our cohort of 871 Japanese patients with PD (430 with sporadic PD and 441 probands with familial PD). Direct sequencing analysis of *LRRK2* revealed 1 proband (0.11%) with a p.R1441G mutation, identified for the first time in Asian countries, besides frequently reported substitutions including, the p.G2019S mutation (0.11%) and p.G2385R variant (11.37%). Several studies have suggested that the *LRRK2* p.R1441G mutation, which is highly prevalent in the Basque country, is extremely rare outside of northern Spain. Further analysis of family members of the proband with the p.R1441G mutation revealed that her mother and first cousin shared the same mutation and parkinsonism. Haplotype analysis revealed a different haplotype from that of the original Spanish families. Our patients demonstrated levodopa-responsive parkinsonism with intrafamilial clinical heterogeneity. This is the first report of familial PD because of the *LRRK2* p.R1441G mutation in Asia.

1. Introduction

Leucine-rich repeat kinase 2 (*LRRK2*) is one of the causative genes of autosomal dominant Parkinson's disease (PD) (Paisan-Ruiz et al., 2004; Zimprich et al., 2004). To date, 7 mutations in *LRRK2* p.G2019S, p.I2020T, p.N1437H, p.R1441G/C/H, and p.Y1699C have been proven as pathogenic mutations. Although p.G2019S and p.R1441G/C/H are frequent mutations in *LRRK2* and the prevalence of the p.G2019S mutation, the most common *LRRK2* substitution in populations of European origin, is estimated at 5%–13% of individuals with familial PD (Haugarvoll and Wszolek, 2009), the p.R1441C, p.R1441H, and p.G2019S mutations have been found to be very rare in Asia (Haugarvoll et al., 2008; Ross et al., 2009). The p.R1441G mutation is frequent in Spain, and especially in the Basque country, where it accounts for 16% of familial and 4% of sporadic cases (Haugarvoll and Wszolek, 2009). However, p.R1441G carriers are extremely rare outside of Spain (Haugarvoll and Wszolek, 2009; Mata et al., 2005, 2009b; Simon-Sanchez et al., 2006). To date, only 4 probands with p.R1441G outside of northern Spain have been reported (Cornejo-Olivas et al., 2013; Deng et al., 2006; Mata et al., 2009a; Yescas et al., 2010). Interestingly, most of the reported p.R1441G PD patients share a common founder, and this mutation is regarded as a rare haplotype (Haugarvoll and Wszolek, 2009; Mata et al., 2005, 2009b; Simon-Sanchez et al., 2006). It remains unclear whether there are patients carrying the p.R1441G mutation in Asia. In this study, we performed a mutation screening of exons 31, 41, and 48 of *LRRK2* in a Japanese cohort of PD patients and found a proband with the p.R1441G mutation. Here, we report the results of a

* Corresponding authors at: Department of Neurology, Juntendo University School of Medicine, 2-1-1 Hongo, Bunkyo-ku, Tokyo 113-8421, Japan. Tel.: +81 3 3813 3111; fax: +81 3 5800 0547.
E-mail addresses: thatano@juntendo.ac.jp (T. Hatano), nhattori@juntendo.ac.jp (N. Hattori).

0197-4580/$ – see front matter © 2014 Elsevier Inc. All rights reserved.
http://dx.doi.org/10.1016/j.neurobiolaging.2014.05.025

clinicoradiological and haplotype analysis of the first familial PD patients linked to p.R1441G mutation in Asian countries.

2. Methods

2.1. Subjects

We studied 871 Japanese PD patients (430 patients with sporadic PD and 441 probands with familial PD; age, 56.4 ± 14.5 years; age at onset, 49.8 ± 14.6 years; disease duration; 6.67 ± 6.89 years). A clinical diagnosis of PD was determined by the presence of at least 2 of 3 cardinal signs (rest tremor, bradykinesia, and rigidity) and improvement following adequate dopaminergic therapy (when available). In this study, families with 2 or more affected members or 2 members with a mutation in at least 2 generations were classified as autosomal dominant PD families, and families with at least 2 affected siblings in only 1 generation were classified as (potential or pseudo-) autosomal recessive PD families. Written informed consent was obtained from all participants, and the local ethics authorities approved the project. A 2-generation pedigree was established for the Japanese family with the *LRRK2* p.R1441G mutation (Fig. 1A). Among the 12 subjects in the family, 4 (II:5, II:4, I:6, and II:2) were willing to participate in this clinicogenetic study, whereas the remainder, including 2 reportedly parkinsonian subjects (I:2 and I:3), refused to participate. Participating individuals were examined by neurologists specializing in movement disorders. A full history was collected and a neurologic examination was performed for each patient.

2.2. Genetic analysis

Genomic DNA from each subject was extracted from peripheral blood using the QIAamp DNA Blood Maxi Kit (QIAGEN, Valencia, CA, USA). Three exons of *LRRK2* that have been frequently reported to contain PD-associated mutations (exons 31, 41, and 48) were analyzed by polymerase chain reaction-direct sequencing using the Big Dye Terminator v.1.1 Cycle Sequencing Kit (Life Technologies, Foster City, CA, USA) as previously described (Zimprich et al., 2004). Haplotype analysis of *LRRK2* flanking region was performed using previously described methods (Mata et al., 2005, 2009a, 2009b).

3. Results

3.1. Genetic findings

In this cohort, we identified 1 proband (0.11%) with a p.R1441G mutation, 1 with a p.G2019S mutation (0.11%), and 103 with a p.G2385R variant (11.37%). We failed to detect p.R1441C, p.R1441H, or p.I2020T mutations in this cohort.

The pedigree of the family with the p.R1441G mutation is shown in Fig. 1A. Five members of this family presented with parkinsonism (I:2, I:3, I:6, II:2, and II:5). Direct sequencing analysis of *LRRK2* revealed a heterozygous p.R1441G (*LRRK2* 4321C>G) mutation in II:5 (proband), I:6, and II:2. A healthy brother (II:4) of the proband did not share the mutation (Fig. 1B). Two individuals (II:2: a first cousin of the proband with the p.R1441G mutation, 50-year-old female; and II:4: a healthy brother of the proband without the p.R1441G mutation, 35-year-old male) were heterozygous for the p.G2385R (*LRRK2* 7153G>A) variant, which was observed on a different haplotype to that in individuals with the p.R1441G mutation. These results show co-segregation of parkinsonism and the mutation in the family, although the remaining members were unable to be tested.

Genotypes for 15 markers from our patients (II:2 and II:5) and the corresponding haplotype shared among 29 p.R1441G carriers from Spanish families are presented in Table 1. Allele sharing was evident at only 3 of the 15 markers and was not observed at c.4937T>C (p.M1646T), a rare polymorphism immediately flanking c.4321C>G (p.R1441G). Thus, our Japanese family members do not share a common founder with the Spanish families.

3.2. Case reports

The clinicoradiological findings in these patients are summarized in Table 2.

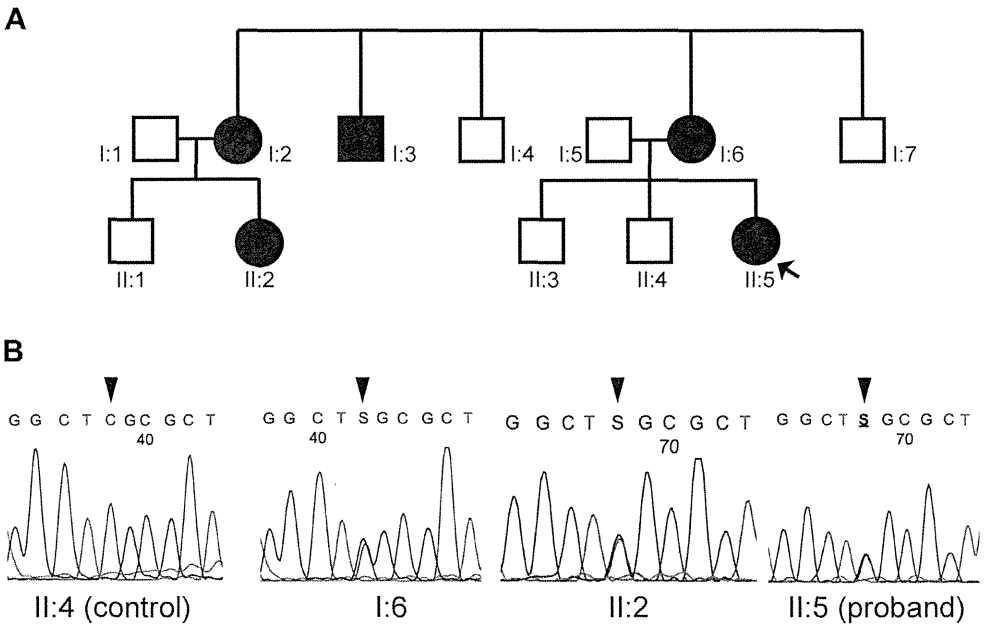

Fig. 1. Pedigree and direct sequencing analysis of the Japanese family with the *LRRK2* p.R1441G mutation. (A) Pedigree of the Japanese family with the *LRRK2* p.R1441G mutation. The arrow indicates the proband. (B) Direct sequencing analysis of *LRRK2* in this family. Arrow heads indicate sites of heterozygous substitution of *LRRK2* 4321C>G.

Table 1
Comparison of R1441G-containing haplotypes across the *LRRK2* region

Location	Marker	Spanish-Basque	Uruguay	II:2	II:5
33305760	D12S2080	**188**	**188**/192	192	192
34142287	rs1511547	**T**	C	C	C
34142413	rs55917927	**C**	T	T	T
34142467	rs56260627	**A**	G	G	G
37708307	rs10876410	**A**	**A**	**A**	**A**
38738007	D12S2194	**249**	253/257	253	253
LRRK2	D12S2516	**252**	254	**252**/254	**252**/254
	R1441 G	**G**	**G**/C	**G**/C	**G**/C
	M1646 T	**C**	T	T	T
	D12S2518	**154**	**154**	**154**	**154**
39116885	D12S2519	**138**	132/140	132/140	132/140
39120098	D12S2520	**248**	257	257	257
39128754	D12S2521	**323**	319/359	315	315
39132380	D12S2522	**281**	283/297	283/297	283/297
39176380	D12S2517	**184**	188/198	202	202
39312730	D12S1048	**211**	**211**/214	220	220

"Spanish-Basque" indicates the haplotype shared among patients with the *LRRK2* p.R1441G mutation from northern Spain. In the members of Japanese family, allele sharing was observed at only 5 markers, indicated in bold.

3.2.1. p.R1441G-Patient II:5

This 36-year-old female developed clumsiness in the right hand and leg at the age of 34 years. Subsequently, she developed right leg tremor and gait disturbance. She did not have any problems with cognition, sleep, or bowel movements. Neurologic examination revealed hemiparkinsonism including resting tremor, muscular rigidity, and akinesia in her right upper and lower limbs along with hyperreflexia in all extremities. Her motor score on the unified PD rating scale (UPDRS part III) was 17 points (Supplementary Video 1). Neurocognitive assessments, such as the Mini Mental State Examination, Frontal Assessment Battery (FAB), and the Japanese version of the Montreal cognitive assessment (MoCA-J) were normal. The odor stick identification test for Japanese revealed mild hyposmia. The administration of levodopa/benserazide (200 mg/50 mg), pramipexole (4 mg), and selegiline (5 mg) resulted in a marked amelioration of her parkinsonism without psychiatric problems. After treatment, her UPDRS part III score was 4 points. Although she did not have any cerebrovascular risk factors, fluid level attenuated inversion recovery (FLAIR) magnetic resonance imaging (MRI) revealed bilateral scattered deep white matter lesions with no structural abnormality (Fig. 2C–F). The results of iodine-123 metaiodobenzylguanidine (^{123}I-MIBG) myocardial scintigraphy were normal (Fig. 2B). Iodine-123 iodoamphetamine single photon emission computed tomography (^{123}I-IMP SPECT) revealed normal regional cerebral blood flow (rCBF) (Fig. 2A).

3.2.2. p.R1441G-Patient I:6

This 65-year-old female is the mother of Patient II:5. Her sister (I:2) and brother (I:3) were also diagnosed as having PD in middle age with no detailed history obtained. She had a history of depression, insomnia over the past 12 years, and right frontoparietal traumatic injury at the age of 55 years. At the age of 60 years, sulpiride (150 mg/d) was administrated for depression, resulting in the development of parkinsonism. Cessation of sulpiride ameliorated her parkinsonism and brotizolam (0.25 mg/d), paroxetine (10 mg/d), zolpidem (5 mg/d), flunitrazepam (2 mg/d), etizolam (1.5 mg/d), and trazodone (50 mg/d) were given for the treatment of her depression and insomnia. At the age of 65 years, she impulsively attempted suicide. The administration of perospirone (12 mg/d) induced a marked deterioration of her motor and swallowing functions. After cessation of perospirone, quetiapine (37.5 mg/d) was used to treat her psychiatric symptoms without aggravation of motor function. Three weeks after the suicide attempt, neurologic examinations revealed minimal left-dominant parkinsonism (Supplementary Video 2) and mild hyposmia (odor stick identification test for Japanese; 6 points).

Although she did not have any problems with orientation, memory, and calculation, the FAB and MoCA-J revealed dysfunctions of verbal fluency and conceptualization (FAB and MoCA-J scores of 14/18 and 24/30, respectively). Although she did not have any cerebrovascular risk factors, T2-weighted, and FLAIR MRI revealed frontotemporal atrophy and small abnormal high intensity lesions in the bilateral frontal white matter (Fig. 2I–L). The results of ^{123}I-MIBG myocardial scintigraphy were normal (Fig. 2H). ^{123}I-IMP SPECT showed decreased rCBF in the bilateral frontal lobes, corresponding to the cranial MRI (Fig. 2G).

3.2.3. p.R1441G-Patient II:2

This 50-year-old female is a first cousin of Patient II:5. She carries both p.R1441G and p.G2385R mutations in *LRRK2*. She had panic syndrome at the age of 18 years. She developed bradykinesia and tremor in the left lower limb at the age of 28 years. On neurologic examination, 2 years after disease onset, she showed left hemiparkinsonism and hyperreflexia in all extremities without any cognitive dysfunction. The administration of levodopa/carbidopa (200 mg/20 mg), trihexyphenidyl (3 mg), talipexole (2.4 mg), and pergolide (0.3 mg) resulted in a marked amelioration of her parkinsonism. Cranial FLAIR MRI was normal and ^{123}I-IMP SPECT showed decreased rCBF in the right basal ganglia (Fig. 2M–O). After the third year of her illness, she developed motor fluctuations with severe ballistic dyskinesia in the left lower limb as a result of high doses of anti-parkinsonian medications. After the 11th year of her illness, bilateral deep brain stimulation of the subthalamic nucleus (STN-DBS) was performed (Fig. 2P). Although STN-DBS was able to temporarily ameliorate her motor complications, she developed dystonic motor complications owing to right-sided STN-DBS stimulation 3 months after the commencement of DBS. In addition, she showed schizophrenic psychosis with severe delusions associated with STN-DBS at 1 year after the operation. After the 13th year of illness, she showed severe wearing off and dyskinesia with off-time pain and dopamine dysregulation syndrome. The left-sided STN-DBS partially ameliorated her off-phase painful dystonia, but caused severe dyskinesia in the on-phase. Eventually, she was put on levodopa/benserazide (700 mg/175 mg/d) and quetiapine (25 mg/d) using left-side STN-DBS in the off-phase only, enabling her to enjoy bowling and ride a bicycle in the on-phase. However, in the off-phase, she showed severe akinesia and panic attacks with delusional ideation.

3.2.4. Other mutations

A 58-year-old male with PD due to p.G2019S, whose father and 2 of 5 siblings had PD developed levodopa-responsive parkinsonism, including resting tremor, rigidity, postural instability, and right lower-limb akinesia without cognition and autonomic dysfunctions. The results of ^{123}I-MIBG myocardial scintigraphy were normal. ^{123}I-IMP SPECT showed decreased rCBF in the frontal lobe, basal ganglia, and bilateral thalamus (Table 2).

Approximately 80% of patients with the p.G2385R variant showed typical parkinsonism with levodopa effectiveness. Autonomic dysfunction is present in <20% of them. In 60% of them, the results of ^{123}I-MIBG myocardial scintigraphy were normal (Table 2).

4. Discussion

Here, we report for the first time an *LRRK2* p.R1441G mutation in Asia. Whereas the p.R1441G mutation is the most prevalent mutation in the Basque country, it is extremely rare outside of northern Spain (Haugarvoll and Wszolek, 2009; Marti-Masso et al.,

Table 2
Clinical features of patients with *LRRK2* p.R1441G mutation

	p.R1441G our cohort			p.G2019S our cohort	p.G2385R our cohort	p.R1441G northern Spain	p.R1441G Uruguay	iPD
	Patient II:5	Patient I:6	Patient II:2					
Age at onset (y)	34	55	28	54	52 (21–83)	55 (29–80)	50	Around 60
Disease duration (y)	2	10	16	4	7		4	
Resting tremor	+	–	+	+	59%	+	+	+
Bradykinesia	+	+	+	+	86.7%	+	+	+
Rigidity	+	+	+	+	82.9%	+	+	+
Gait disturbance	+	–	+	+	80%	+	N.A.	+
Postural instability	–	–	+	+	62.9%	+	+	+
Clinical response to levodopa	+	N.A.	+	+	69.5%	+	+	+
Wearing off	–	–	+	N.A.	28.6%	+	N.A.	+
Levodopa-induced dyskinesia	–	–	+	N.A.	24.8%	+	N.A.	+
Asymmetry at onset	+	+	+	+	73.3%	+	+	+
Hyposmia (OSIT-J)	Mild impairment (9, cutoff; 11.09[a])	Mild impairment (6, cutoff; 9.78[a])	N.A.	N.A.	N.A.	Mild impairment	N.A.	Severe impairment
Orthostatic hypotension	–	–	–	–	12.4%	–	N.A.	+
Incontinence	–	–	–	–	18.1%	–	N.A.	+
Sleep benefit	+	–	Unknown	–	16.2%	–	N.A.	–
Dystonia at onset	–	–	–	N.A.	14.3%	–	N.A.	–
Hyperreflexia	+	–	+	N.A.	17.1%	–	N.A.	–
Hallucination	–	–	+	–	16.2%	–	N.A.	–
Dementia (FAB/MMSE/MoCA-J)	– (18/30/29)	Slt. frontal dysfunction (14/N.A./24)	–	–	12.4%	–	–	–
Other psychiatric problems	–	Depression, executive dysfunction	S-like, delusion	–	±	±	N.A.	–
Brain MRI	Abnormal small spots scatter in white matter	Abnormal small spots scatter in white matter, bilateral frontal lobe atrophy, post traumatic hemorrhage in right frontoparietal cortex	No abnormality	N.A.	N.A.	No abnormality	N.A.	No abnormality
^{123}I-IMP SPECT	Normal record	Decreased rCBF in bil. frontal lobes	Decreased rCBF in the right basal ganglia	Decreased rCBF in frontal, basal ganglia, and right thalamus	N.A.	N.A.	N.A.	Decreased rCBF in bil. occipital lobes
^{123}I-MIBG myocardiac scintigraphy	H/M ratio (E/L) = 2.38/2.68; cutoff, 1.4[b]; wash out ratio= 4.15%	H/M ratio (E/L) = 3.18/3.63; cutoff, 2.0[b]; wash out ratio = 20.1%	Not performed	Normal	Decreased 40%, normal 60%	Less decreased than PD	N.A.	Decreased H/M ratio

Key: Bil., bilateral; H/M, heart/mediastinum ratio; FAB, frontal assessment battery; ^{123}I-MIBG, iodine-123 metaiodobenzylguanidine; iPD, idiopathic Parkinson's disease; MMSE, mini mental state examination; MoCA-J, Japanese version of the Montreal cognitive assessment; MRI, magnetic resonance imaging; N.A., not applicable; OSIT-J, odor stick identification test for Japanese; PD, Parkinson's disease; rCBF, regional cerebral blood flow; S-like, schizophrenic-like; Slt., slightly.

[a] Cutoff points in OSIT-J vary according to age and sex.

[b] Cutoff points in ^{123}I-MIBG myocardiac scintigraphy were different in every institution.

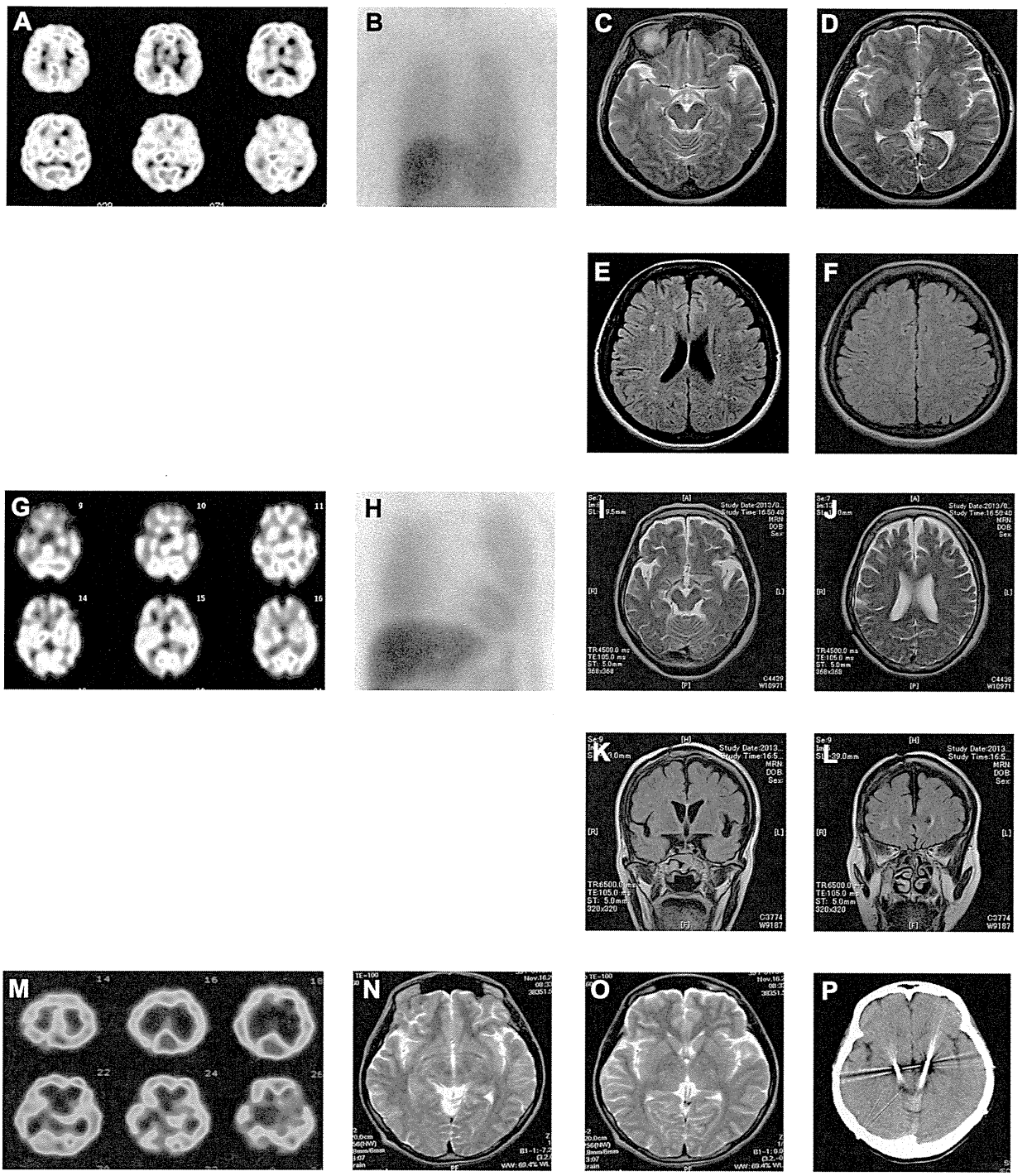

Fig. 2. Cranial MRI, CT, ^{123}I-IMP SPECT, and ^{123}I-MIBG myocardial scintigraphy of Patients II:5, I:6, and II:2. In Patient II:5, ^{123}I-IMP SPECT and ^{123}I-MIBG myocardial scintigraphy show no abnormality (A, B). Cranial T2-WI and FLAIR MRI depict several abnormal high-intensity lesions without any atrophy (C–F). In Patient I:6, ^{123}I-IMP SPECT shows hypoperfusion of bilateral frontal area (G). Cranial T2-WI and FLAIR MRI show several abnormal high-intensity lesions with frontal lobe atrophy (I–L). The results of ^{123}I-MIBG myocardial scintigraphy were normal (E). In Patient II:2, ^{123}I-IMP SPECT shows hypoperfusion of the right basal ganglia (M). Cranial T2-WI MRI showing no abnormality (O, P). Cranial CT showed that electrodes for deep brain stimulation of the subthalamic nucleus were implanted into the bilateral subthalamic nucleus (N). Abbreviations: CT, computerized tomography; FLAIR, fluid level attenuated inversion recovery; ^{123}I-IMP SPECT, Iodine-123 iodoamphetamine single photon emission computed tomography; ^{123}I-MIBG, iodine-123 metaiodobenzylguanidine; MRI, magnetic resonance imaging.

2009; Mata et al., 2005, 2009b; Simon-Sanchez et al., 2006). In our family, the lack of sharing at p.M1646T (Table 1), located 9.7 kb downstream from the mutation, is particularly informative because the "*LRRK2* c.4937 T>C" allele occurs at a frequency of <2% in controls from northern Spain but has been observed in all mutation carriers described in the literature (Mata et al., 2005). Therefore, we concluded that our family has a different haplotype from that of all the Spanish families reported to date. Recently, a cohort study revealed a Uruguayan patient carrying a p.R1441G mutation, who did not share the haplotype of the original Spanish

families (Mata et al., 2009a). Our patients did not appear to have an ancestor from outside Japan based on historical records. Thus, they are only the second family with this mutation outside of Spain, with a different haplotype, reinforcing the hypothesis that p.R1441 is a mutational hot spot. It is therefore possible that patients with a mutation at *LRRK2* p.R1441 are distributed worldwide.

Previous reports have described that the clinical features of the original Basque family members (Paisan-Ruiz et al., 2005) and the Uruguayan patient (Mata et al., 2009a) with *LRRK2* p.R1441G were similar to those of typical idiopathic PD (iPD), including good response to levodopa therapy, rigidity, and akinesia (Table 2). Although most of the members of the Basque families showed late-onset PD (Gonzalez-Fernandez et al., 2007; Mata et al., 2005; Simon-Sanchez et al., 2006), Gonzalez-Fernandez et al. (2007) reported that 5 of 15 patients showed an early age at onset (<50 years). These findings indicate that some of the Basque families might exhibit intrafamilial clinical heterogeneity. In our Japanese family, Patients II:2 and II:5 also showed younger age at onset compared with iPD patients. In contrast to Patients I:2, I:3, II:2, and II:5, Patient I:6, albeit in old age, showed trivial hemiparkinsonism only detected by detailed neurologic examination with no functional disabilities, whereas the patient showed frontal dysfunction with impaired verbal fluency and conceptualization. Severe psychosis appeared to be unique to Patient II:2 in our family. Therefore, our family also exhibited intrafamilial clinical heterogeneity. The presence of such heterogeneity suggests that additional factors, that is, genetic and/or environmental factors, contribute to the development of the disease in association with the p.R1441G mutation.

Based on the results of 2 studies, patients with the *LRRK2* p.R1441G mutation seem to display fewer of the non-motor features characteristic of iPD, such as hyposmia and cardiac sympathetic denervation (Table 2) (Ruiz-Martinez et al., 2011; Tijero et al., 2013). Consistent with these observations, our patients showed no autonomic dysfunctions, including bowel and urinary dysfunctions and orthostatic hypotension, REM-sleep behavior disorders, or reduced cardiac ^{123}I-MIBG uptake (Table 2). Hyposmia detected in our patients (II:5 and I:6) appeared less severe than that in iPD, requiring further studies to determine whether the p.R1441G mutation is associated with hyposmia. In terms of neuroimaging, we also observed differences between patients with the p.R1441G mutation and iPD patients. Patient I:6 showed frontal atrophy on MRI and frontal hypoperfusion on ^{123}I-IMP SPECT. Furthermore, ^{123}I-IMP SPECT of Patient II:2 revealed hypoperfusion in the basal ganglia. These findings contrast with those in iPD patients, which typically show a decrement of blood flow in the occipital lobes (Abe et al., 2003). On the basis of these results, the phenotypes of our patients seemed to be different from those of iPD patients with Lewy pathology. Pathologic findings in PD patients with *LRRK2* mutations are very variable despite them exhibiting a relatively uniform clinical phenotype of parkinsonism (Cookson et al., 2008; Hasegawa et al., 2009; Ross et al., 2006; Ujiie et al., 2012; Zimprich et al., 2004). A clinicopathological study of patients with the p.G2019S mutation revealed no correlation between Lewy pathology and clinical phenotypes, including dementia and psychiatric symptoms (Ross et al., 2006). These observations suggest that additional factors besides LRRK2 mutations could play roles in the development of dementia and/or psychiatric problems as well as Lewy pathology. It therefore remains to be clarified whether our cases show Lewy pathology, although a previously reported patient with a p.R1441G mutation did not have Lewy pathology (Marti-Masso et al., 2009).

It has been described that the phenotype of PD patients with the p.G2019S mutation cannot be distinguished from iPD (Haugarvoll and Wszolek, 2009). However, the patient with the p.G2019S mutation in our cohort showed no autonomic dysfunction, no psychosis, no dementia, and normal cardiac ^{123}I-MIBG uptake, resembling the phenotype of p.R1441G-patient II:5 without early age of onset. The prevalence of autonomic dysfunctions of PD patients with p.G2385R was also seemed to be less than that in iPD patients (Khoo et al., 2013). Two members (II:2 and II:4) of our family also had the p.G2385R variant. Although combining p.R1441G with p.G2385R in II:2 might cause severe psychosis, it remains unclear whether the p.G2385R variant combined with an LRRK2 pathogenic mutation might be associated with a deterioration of clinical phenotypes. Therefore, we could not determine the contribution of this variant to the phenotypic modifications in our family.

In Patient II:2, STN-DBS exacerbated psychiatric problems without any improvement of motor function. Gomez-Esteban et al. (2008) also described a poor response to STN-DBS therapy in patients with the p.R1441G mutation. These results might be attributable to the p.R1441G mutation.

We found 1 patient with the p.G2019S mutation (0.11%) in this cohort. Parkinsonism because of p.G2019S is common in Caucasian populations (Haugarvoll and Wszolek, 2009), and the frequencies in the Ashkenazi Jewish and North African Arab cohorts are 18.3% and 39%, respectively (Lesage et al., 2006; Ozelius et al., 2006). However, this mutation has been reported to be very rare in Asian populations (Tan et al., 2005; Tomiyama et al., 2006; Zabetian et al., 2006), consistent with our cohort. The finding of a relatively high prevalence of the *LRRK2* p.G2385R variant in our cohort is consistent with the findings of previous reports (Funayama et al., 2007; Ross et al., 2011). Although Ross et al. (2011) described that the prevalence of PD with p.G2385R in large Asian populations, including Japanese was about 3%, the prevalence of p.G2385R in the previously reported Japanese cohort was 11.6% (Funayama et al., 2007), similar to that in the present cohort. On the other hand, the association of p.G2385R with PD in the Caucasian population was not supported by the results of a previous large population study (Ross et al., 2011).

To the best of our knowledge, this is the first report of an *LRRK2* p.R1441G mutation in Asia and only the third outside of northern Spain (Mata et al., 2009a). Further mutation screening of *LRRK2* p.R1441G in Asian populations may confirm the characteristic features of patients with this mutation.

Disclosure statement

The authors report no conflicts of interest and have no financial interest related to the material described in the manuscript.

Acknowledgements

The authors thank Dr Hideo Mori (Juntendo Koshigaya Hospital) and all the participants in this study. This work was supported by a Strategic Research Foundation Grant-in-Aid Project for Private Universities, Grants-in-Aid for Scientific Research (KAKENHI) (to Nobutaka Hattori, 24390224 and to Taku Hatano, 25461290) and a Grant-in-Aid for Scientific Research on Innovative Areas (to Nobutaka Hattori, 23111003 and to Manabu Funayama, 25129707) from the Japanese Ministry of Education, Culture, Sports, Science and Technology. This work was also supported by grants from the Parkinson's Disease Foundation, United States and the National Institutes of Health, United States (R01 NS065070 and P50 NS062684).Appendix A. Supplementary dataSupplementary Video 1. Supplementary Video 2.

Appendix A. Supplementary data

Supplementary data associated with this article can be found, in the online version, at http://dx.doi.org/10.1016/j.neurobiolaging.2014.05.025.

References

Abe, Y., Kachi, T., Kato, T., Arahata, Y., Yamada, T., Washimi, Y., Iwai, K., Ito, K., Yanagisawa, N., Sobue, G., 2003. Occipital hypoperfusion in Parkinson's disease without dementia: correlation to impaired cortical visual processing. J. Neurol. Neurosurg. Psychiatry 74, 419–422.

Cookson, M.R., Hardy, J., Lewis, P.A., 2008. Genetic neuropathology of Parkinson's disease. Int. J. Clin. Exp. Pathol. 1, 217–231.

Cornejo-Olivas, M.R., Torres, L., Mazzetti, P., Cosentino, C., Zabetian, C.P., Mata, I.F., 2013. Variable penetrance of the LRRK2-R1441G mutation in a Peruvian family [abstract]. Mov. Disord. 23 (Suppl. 1), 1154.

Deng, H., Le, W., Guo, Y., Hunter, C.B., Xie, W., Huang, M., Jankovic, J., 2006. Genetic analysis of LRRK2 mutations in patients with Parkinson disease. J. Neurol. Sci. 251, 102–106.

Funayama, M., Li, Y., Tomiyama, H., Yoshino, H., Imamichi, Y., Yamamoto, M., Murata, M., Toda, T., Mizuno, Y., Hattori, N., 2007. Leucine-rich repeat kinase 2 G2385R variant is a risk factor for Parkinson disease in Asian population. Neuroreport 18, 273–275.

Gomez-Esteban, J.C., Lezcano, E., Zarranz, J.J., Gonzalez, C., Bilbao, G., Lambarri, I., Rodriguez, O., Garibi, J., 2008. Outcome of bilateral deep brain subthalamic stimulation in patients carrying the R1441G mutation in the LRRK2 dardarin gene. Neurosurgery 62, 857–863.

Gonzalez-Fernandez, M.C., Lezcano, E., Ross, O.A., Gomez-Esteban, J.C., Gomez-Busto, F., Velasco, F., Alvarez-Alvarez, M., Rodriguez-Martinez, M.B., Ciordia, R., Zarranz, J.J., Farrer, M.J., Mata, I.F., de Pancorbo, M.M., 2007. Lrrk2-associated parkinsonism is a major cause of disease in Northern Spain. Parkinsonism Relat. Disord. 13, 509–515.

Hasegawa, K., Stoessl, T., Yokoyama, T., Kowa, H., Wszolek, Z.K., Yagishita, S., 2009. Familial parkinsonism: study of original Sagamihara PARK8 (I2020T) kindred with variable clinicopathologic outcomes. Parkinsonism Relat. Disord. 15, 300–306.

Haugarvoll, K., Wszolek, Z.K., 2009. Clinical features of LRRK2 parkinsonism. Parkinsonism Relat. Disord. 15 (Suppl. 3), S205–S208.

Haugarvoll, K., Rademakers, R., Kachergus, J.M., Nuytemans, K., Ross, O.A., Gibson, J.M., Tan, E.K., Gaig, C., Tolosa, E., Goldwurm, S., Guidi, M., Riboldazzi, G., Brown, L., Walter, U., Benecke, R., Berg, D., Gasser, T., Theuns, J., Pals, P., Cras, P., De Deyn, P.P., Engelborghs, S., Pickut, B., Uitti, R.J., Foroud, T., Nichols, W.C., Hagenah, J., Klein, C., Samii, A., Zabetian, C.P., Bonifati, V., Van Broeckhoven, C., Farrer, M.J., Wszolek, Z.K., 2008. Lrrk2 R1441C parkinsonism is clinically similar to sporadic Parkinson disease. Neurology 70, 1456–1460.

Khoo, T.K., Yarnall, A.J., Duncan, G.W., Coleman, S., O'Brien, J.T., Brooks, D.J., Barker, R.A., Burn, D.J., 2013. The spectrum of nonmotor symptoms in early Parkinson disease. Neurology 80, 276–281.

Lesage, S., Durr, A., Tazir, M., Lohmann, E., Leutenegger, A.L., Janin, S., Pollak, P., Brice, A., French Parkinson's Disease Genetics Study Group, 2006. LRRK2 G2019S as a cause of Parkinson's disease in North African Arabs. N. Engl. J. Med. 354, 422–423.

Marti-Masso, J.F., Ruiz-Martinez, J., Bolano, M.J., Ruiz, I., Gorostidi, A., Moreno, F., Ferrer, I., Lopez de Munain, A., 2009. Neuropathology of Parkinson's disease with the R1441G mutation in LRRK2. Mov. Disord. 24, 1998–2001.

Mata, I.F., Taylor, J.P., Kachergus, J., Hulihan, M., Huerta, C., Lahoz, C., Blazquez, M., Guisasola, L.M., Salvador, C., Ribacoba, R., Martinez, C., Farrer, M., Alvarez, V., 2005. LRRK2 R1441G in Spanish patients with Parkinson's disease. Neurosci. Lett. 382, 309–311.

Mata, I.F., Cosentino, C., Marca, V., Torres, L., Mazzetti, P., Ortega, O., Raggio, V., Aljanati, R., Buzo, R., Yearout, D., Dieguez, E., Zabetian, C.P., 2009a. LRRK2 mutations in patients with Parkinson's disease from Peru and Uruguay. Parkinsonism Relat. Disord. 2009, 370–373.

Mata, I.F., Hutter, C.M., Gonzalez-Fernandez, M.C., de Pancorbo, M.M., Lezcano, E., Huerta, C., Blazquez, M., Ribacoba, R., Guisasola, L.M., Salvador, C., Gomez-Esteban, J.C., Zarranz, J.J., Infante, J., Jankovic, J., Deng, H., Edwards, K.L., Alvarez, V., Zabetian, C.P., 2009b. Lrrk2 R1441G-related Parkinson's disease: evidence of a common founding event in the seventh century in Northern Spain. Neurogenetics 10, 347–353.

Ozelius, L.J., Senthil, G., Saunders-Pullman, R., Ohmann, E., Deligtisch, A., Tagliati, M., Hunt, A.L., Klein, C., Henick, B., Hailpern, S.M., Lipton, R.B., Soto-Valencia, J., Risch, N., Bressman, S.B., 2006. LRRK2 G2019S as a cause of Parkinson's disease in Ashkenazi Jews. N. Engl. J. Med. 354, 424–425.

Paisan-Ruiz, C., Jain, S., Evans, E.W., Gilks, W.P., Simon, J., van der Brug, M., Lopez de Munain, A., Aparicio, S., Gil, A.M., Khan, N., Johnson, J., Martinez, J.R., Nicholl, D., Carrera, I.M., Pena, A.S., de Silva, R., Lees, A., Marti-Masso, J.F., Perez-Tur, J., Wood, N.W., Singleton, A.B., 2004. Cloning of the gene containing mutations that cause PARK8-linked Parkinson's disease. Neuron 44, 595–600.

Paisan-Ruiz, C., Saenz, A., Lopez de Munain, A., Marti, I., Martinez Gil, A., Marti-Masso, J.F., Perez-Tur, J., 2005. Familial Parkinson's disease: clinical and genetic analysis of four Basque families. Ann. Neurol. 57, 365–372.

Ross, O.A., Toft, M., Whittle, A.J., Johnson, J.L., Papapetropoulos, S., Mash, D.C., Litvan, I., Gordon, M.F., Wszolek, Z.K., Farrer, M.J., Dickson, D.W., 2006. Lrrk2 and Lewy body disease. Ann. Neurol. 59, 388–393.

Ross, O.A., Spanaki, C., Griffith, A., Lin, C.H., Kachergus, J., Haugarvoll, K., Latsoudis, H., Plaitakis, A., Ferreira, J.J., Sampaio, C., Bonifati, V., Wu, R.M., Zabetian, C.P., Farrer, M.J., 2009. Haplotype analysis of Lrrk2 R1441H carriers with parkinsonism. Parkinsonism Relat. Disord. 15, 466–467.

Ross, O.A., Soto-Ortolaza, A.I., Heckman, M.G., Aasly, J.O., Abahuni, N., Annesi, G., Bacon, J.A., Bardien, S., Bozi, M., Brice, A., Brighina, L., Van Broeckhoven, C., Carr, J., Chartier-Harlin, M.C., Dardiotis, E., Dickson, D.W., Diehl, N.N., Elbaz, A., Ferrarese, C., Ferraris, A., Fiske, B., Gibson, J.M., Gibson, R., Hadjigeorgiou, G.M., Hattori, N., Ioannidis, J.P., Jasinska-Myga, B., Jeon, B.S., Kim, Y.J., Klein, C., Kruger, R., Kyratzi, E., Lesage, S., Lin, C.H., Lynch, T., Maraganore, D.M., Mellick, G.D., Mutez, E., Nilsson, C., Opala, G., Park, S.S., Puschmann, A., Quattrone, A., Sharma, M., Silburn, P.A., Sohn, Y.H., Stefanis, L., Tadic, V., Theuns, J., Tomiyama, H., Uitti, R.J., Valente, E.M., van de Loo, S., Vassilatis, D.K., Vilarino-Guell, C., White, L.R., Wirdefeldt, K., Wszolek, Z.K., Wu, R.M., Farrer, M.J., Genetic Epidemiology Of Parkinson's Disease, Consortium, 2011. Association of *LRRK2* exonic variants with susceptibility to Parkinson's disease: a case–control study. Lancet Neurol. 10, 898–908.

Ruiz-Martinez, J., Gorostidi, A., Goyenechea, E., Alzualde, A., Poza, J.J., Rodriguez, F., Bergareche, A., Moreno, F., Lopez de Munain, A., Marti Masso, J.F., 2011. Olfactory deficits and cardiac 123I-MIBG in Parkinson's disease related to the LRRK2 R1441G and G2019S mutations. Mov. Disord. 26, 2026–2031.

Simon-Sanchez, J., Marti-Masso, J.F., Sanchez-Mut, J.V., Paisan-Ruiz, C., Martinez-Gil, A., Ruiz-Martinez, J., Saenz, A., Singleton, A.B., Lopez de Munain, A., Perez-Tur, J., 2006. Parkinson's disease due to the R1441G mutation in Dardarin: a founder effect in the Basques. Mov. Disord. 21, 1954–1959.

Tan, E.K., Shen, H., Tan, L.C., Farrer, M., Yew, K., Chua, E., Jamora, R.D., Puvan, K., Puong, K.Y., Zhao, Y., Pavanni, R., Wong, M.C., Yih, Y., Skipper, L., Liu, J.J., 2005. The G2019S LRRK2 mutation is uncommon in an Asian cohort of Parkinson's disease patients. Neurosci. Lett. 384, 327–329.

Tijero, B., Gomez Esteban, J.C., Somme, J., Llorens, V., Lezcano, E., Martinez, A., Rodriguez, T., Berganzo, K., Zarranz, J.J., 2013. Autonomic dysfunction in parkinsonian LRRK2 mutation carriers. Parkinsonism Relat. Disord. 19, 906–909.

Tomiyama, H., Li, Y., Funayama, M., Hasegawa, K., Yoshino, H., Kubo, S.I., Sato, K., Hattori, T., Lu, C.S., Inzelberg, R., Djaldetti, R., Melamed, E., Amouri, R., Gouider-Khouja, N., Hentati, F., Hatano, Y., Wang, M., Imamichi, Y., Mizoguchi, K., Miyajima, H., Obata, F., Toda, T., Farrer, M.J., Mizuno, Y., Hattori, N., 2006. Clinicogenetic study of mutations in LRRK2 exon 41 in Parkinson's disease patients from 18 countries. Mov. Disord. 21, 1102–1108.

Ujiie, S., Hatano, T., Kubo, S.I., Imai, S., Sato, S., Uchihara, T., Yagishita, S., Hasegawa, K., Kowa, H., Sakai, F., Hattori, N., 2012. LRRK2 I2020T mutation is associated with tau pathology. Parkinsonism Relat. Disord. 18, 819–823.

Yescas, P., Lopez, M., Monroy, N., Boll, M.C., Rodriguez-Violante, M., Rodriguez, U., Ochoa, A., Alonso, M.E., 2010. Low frequency of common LRRK2 mutations in Mexican patients with Parkinson's disease. Neurosci. Lett. 485, 79–82.

Zabetian, C.P., Morino, H., Ujike, H., Yamamoto, M., Oda, M., Maruyama, H., Izumi, Y., Kaji, R., Griffith, A., Leis, B.C., Roberts, J.W., Yearout, D., Samii, A., Kawakami, H., 2006. Identification and haplotype analysis of LRRK2 G2019S in Japanese patients with Parkinson disease. Neurology 67, 697–699.

Zimprich, A., Biskup, S., Leitner, P., Lichtner, P., Farrer, M., Lincoln, S., Kachergus, J., Hulihan, M., Uitti, R.J., Calne, D.B., Stoessl, A.J., Pfeiffer, R.F., Patenge, N., Carbajal, I.C., Vieregge, P., Asmus, F., Muller-Myhsok, B., Dickson, D.W., Meitinger, T., Strom, T.M., Wszolek, Z.K., Gasser, T., 2004. Mutations in LRRK2 cause autosomal-dominant parkinsonism with pleomorphic pathology. Neuron 44, 601–607.

OPEN ACCESS Freely available online

PLOS ONE

p150^{glued}-Associated Disorders Are Caused by Activation of Intrinsic Apoptotic Pathway

Kei-Ichi Ishikawa[1], Shinji Saiki[1], Norihiko Furuya[1,2], Daisuke Yamada[1], Yoko Imamichi[1], Yuanzhe Li[1], Sumihiro Kawajiri[1], Hironori Sasaki[1], Masato Koike[3], Yoshio Tsuboi[4], Nobutaka Hattori[1,2]*

1 Department of Neurology, Juntendo University School of Medicine, Tokyo, Japan, **2** Department of Research and Therapeutics for Movement Disorders, Juntendo University School of Medicine, Tokyo, Japan, **3** Department of Cell Biology and Neuroscience, Juntendo University School of Medicine, Tokyo, Japan, **4** Department of Neurology, Fukuoka University School of Medicine, Fukuoka, Japan

Abstract

Mutations in p150^{glued} cause hereditary motor neuropathy with vocal cord paralysis (HMN7B) and Perry syndrome (PS). Here we show that both overexpression of p150^{glued} mutants and knockdown of endogenous p150^{glued} induce apoptosis. Overexpression of a p150^{glued} plasmid containing either a HMN7B or PS mutation resulted in cytoplasmic p150^{glued}-positive aggregates and was associated with cell death. Cells containing mutant p150^{glued} aggregates underwent apoptosis that was characterized by an increase in cleaved caspase-3- or Annexin V-positive cells and was attenuated by both zVAD-fmk (a pan-caspase inhibitor) application and caspase-3 siRNA knockdown. In addition, overexpression of mutant p150^{glued} decreased mitochondrial membrane potentials and increased levels of translocase of the mitochondrial outer membrane (Tom20) protein, indicating accumulation of damaged mitochondria. Importantly, siRNA knockdown of endogenous p150^{glued} independently induced apoptosis via caspase-8 activation and was not associated with mitochondrial morphological changes. Simultaneous knockdown of endogenous p150^{glued} and overexpression of mutant p150^{glued} had additive apoptosis induction effects. These findings suggest that both p150^{glued} gain-of-toxic-function and loss-of-physiological-function can cause apoptosis and may underlie the pathogenesis of p150^{glued}-associated disorders.

Citation: Ishikawa K-I, Saiki S, Furuya N, Yamada D, Imamichi Y, et al. (2014) p150^{glued}-Associated Disorders Are Caused by Activation of Intrinsic Apoptotic Pathway. PLoS ONE 9(4): e94645. doi:10.1371/journal.pone.0094645

Editor: Hiroyoshi Ariga, Hokkaido University, Japan

Received December 2, 2013; **Accepted** March 18, 2014; **Published** April 10, 2014

Funding: The authors are grateful for these 9 grants: the Grant from the Japanese Ministry of Health, Labour and Welfare (http://www.mhlw.go.jp/stf/seisakunitsuite/bunya/hokabunya/kenkyujigyou/index.html) (N.H.), the Grant-in-Aid for Young Scientists (A) (S.S.), the Grant-in-Aid for Scientific Research (C) (N.F.), the Grant-in-Aid for Challenging Exploratory Research (S.S.) from Japan Society for the Promotion of Science (http://www.jsps.go.jp/index.html), Grant-in-Aid for Scientific Research on Priority Areas (S.S.) from Japanese Ministry of Education, Culture, Sports, Science and Technology (http://www.mext.go.jp/a_menu/shinkou/hojyo/main5_a5.htm), and grants from the Life Science Foundation (http://www.lifesci-found.com/), the Takeda Scientific Foundation (http://www.takeda-sci.or.jp/), the Cell Science Research Foundation (http://www.shionogi.co.jp/zaidan/), and the Nakajima Foundation (http://www.nakajimafound.or.jp/index.html) (S.S.). The funders had no role in study design, data collection and analysis, decision to publish, or preparation of the manuscript.

Competing Interests: The authors have declared that no competing interests exist.

* E-mail: nhattori@juntendo.ac.jp

Introduction

The dynactin subunit p150^{glued} is encoded by the *DCTN1* gene. Mutations in this gene have been detected in patients with slowly progressive autosomal dominant distal hereditary motor neuropathy with vocal cord paralysis (HMN7B) and autosomal dominant Perry syndrome (PS), the latter of which is characterized by rapidly progressive, devastating neurodegeneration of dopaminergic neurons in the substantia nigra [1,2].

Dynactin has various molecular functions including minus-end vesicular transport, protein degradation, and cell division. p150^{glued} is the largest polypeptide of the dynactin complex, and it binds directly to microtubules and to cytoplasmic dynein. Disruption of the p150^{glued} CAP-Gly domain in neurons causes insufficient retrograde axonal transport [3,4]. Transgenic mice expressing p150^{glued} with a G59S mutation develop progressive degeneration of motor neurons similar to that seen in amyotrophic lateral sclerosis [5–7]. The mutated p150^{glued} polypeptide that causes PS is unable to bind to microtubules and forms intracytoplasmic aggregates. These aggregates include abnormally accumulated mitochondria [11]. Despite these findings, it is unclear whether decreased levels of endogenous p150^{glued} or increased levels of the mutant form dominantly contribute to the neurodegeneration seen in PS.

Here we report that knockdown of endogenous p150^{glued} and overexpression of p150^{glued} with pathogenic HMN7B or PS mutations independently induced apoptosis. However, only overexpression of mutant forms of p150^{glued} induced intracytoplasmic p150^{glued}-aggregates and accumulation of damaged mitochondria, resulting in intrinsic apoptosis induction. Importantly, mutant p150^{glued} overexpression with endogenous p150^{glued} knockdown showed additive effects on apoptosis induction, suggesting that both a gain- and loss-of-function contribute to the disease pathogenesis.

Results

Cells overexpressing various p150^{glued} mutants produce cytoplasmic aggregates

To investigate the effects of overexpression of mutant p150^{glued}, we first generated plasmid DNAs encoding GFP- or 3xFLAG-tagged wild-type (WT) and mutant p150^{glued} with each pathogenic mutation: G59S, which causes HMN7B, and G71A, G71E,

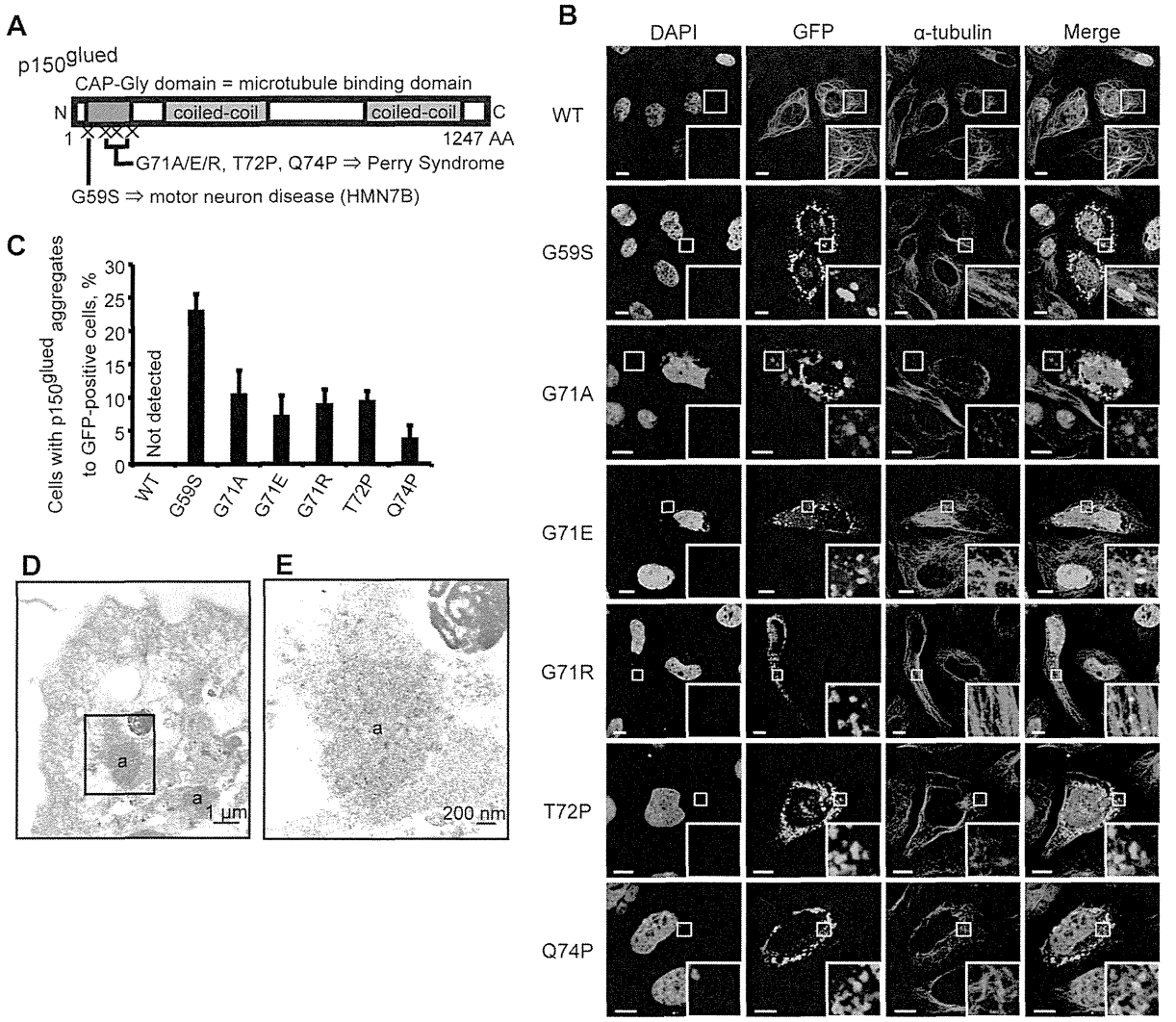

Figure 1. Disease-associated p150^{glued} mutant proteins form aggregates. (A) Schematic of the p150^{glued} subunit of dynactin. (B) HeLa cells transfected with GFP-tagged wild-type or mutant p150^{glued} were fixed and stained with an antibody against α-tubulin (red) after 24 h and analyzed using confocal microscopy. Insets show higher magnification of the boxed areas. Bars, 10 μm. (C) The percentages of GFP-positive cells that contained aggregates are shown. The error bar indicates each standard deviation. Statistics are from three independent experiments. (D, E) Electron micrographic examination of HeLa cells transfected with GFP-tagged G59S p150^{glued} and immunolabeled with an antibody against GFP. (E) High magnification of the boxed area shown in (D). Intracytoplasmic aggregates (a) are labeled.
doi:10.1371/journal.pone.0094645.g001

G71R, T72P, or Q74P, which cause PS. All of these mutations are within the p150^{glued} CAP-Gly microtubule binding domain (Figure 1A).

To determine if a mutation in p150^{glued} affected its intracellular localization, we transfected GFP-tagged WT or mutant p150^{glued} into HeLa cells followed by immunocytochemical analysis. HeLa cells overexpressing GFP-WT p150^{glued} showed complete colocalization with tubulin (Figure 1B). By contrast, those with a pathogenic mutation were diffusely distributed in the cytoplasm and showed no apparent colocalization with tubulin (Figure S1A). Additionally, cytoplasmic, but not nuclear, aggregates were observed in cells with high expression levels of the mutant p150^{glued} plasmids as early as 24 h after transfection, most frequently in the perinuclear region of the cells with G59S p150^{glued} (Figure 1B, C). These findings are consistent with previous reports [8,11]. Analogous results were detected with the overexpression of 3xFLAG-tagged WT and mutant p150^{glued} in SH-SY5Y (Figure S1B) and HeLa cells (Figure S1C, D). Previous studies examining the overexpression of mutant G59S p150^{glued} showed decreased affinity of the mutant form of p150^{glued} for microtubules, indicating that mutant p150^{glued} dissociated from microtubules and formed aggregates [11].

To confirm the formation of cytoplasmic aggregates, we performed conventional electron microscopy (EM) analysis. High-density aggregates around the nuclei were detected in cells overexpressing G59S or G71R p150^{glued} (Figure S1E). Next, using immuno-EM analysis with anti-GFP antibodies to recognize GFP-tagged mutant p150^{glued}, we detected p150^{glued} localized in high

density aggregates, particularly in the perinuclear region of the cells overexpressing G59S (Figure 1D, E) or G71R (data not shown) p150^{glued}. Unfortunately, because of the fixation technique for immuno-EM, we could not use the same specimens to assess morphological changes in organelles, including mitochondria, in the cells that showed the aggregates.

We next sought to determine the characteristics of the aggregates by immunocytochemistry. The mutant p150^{glued} aggregates were partially positive for endogenous ubiquitin but not for FLAG-tagged TAR DNA-binding protein 43 (TDP-43) (Figure S1F, G). This is consistent with previous reports showing that dynactin subunits p50 and p62 were present in less than 5% of TDP-43-expressing neurons in the globus pallidus of the autopsied brain of a PS patient [8].

Apoptotic changes occurred in cells with cytoplasmic aggregates

To elucidate the pathogenesis of the p150^{glued}-associated diseases, we focused on the association of cytoplasmic aggregates induced by mutant p150^{glued} overexpression with cell death. We tested the death rate of cells expressing the GFP-tagged p150^{glued}, assessed by nuclear morphological changes described in a previous report [12]. The rate of cell death was significantly increased by overexpression of G59S or G71R p150^{glued} both 24 and 48 h after transfection when compared with control cells (Figure 2A).

To examine the characteristics of the cell death induced by G59S or G71R p150^{glued}, we performed the same analysis 24 h after transfection with controls cells and cells treated with the pan-caspase inhibitor carbobenzoxy-valyl-alanyl-aspartyl-[O-methyl]-fluoromethylketone (z-VAD-fmk). The rate of cell death induced by overexpression of G59S or G71R p150^{glued} was significantly suppressed by z-VAD (Figure 2B) [13]. In a population of cells selected based on GFP (p150^{glued}) intensity, the numbers of early apoptotic cells (annexin V-positive, propidium iodide (PI)-negative) and late apoptotic or necrotic cells (annexin V-positive, PI-positive) were both increased by overexpression of G59S or G71R p150^{glued} (Figure 2C, D). Likewise, z-VAD treatment significantly decreased cell death in both G59S and G71R p150^{glued}-overexpressing cells.

To examine the activation of the intrinsic apoptotic pathway, we determined whether or not cells with aggregates were positive for cleaved caspase-3 using fluorescent-activated cell sorting (FACS) and immunocytochemistry analyses. The number of cells positive for both cleaved caspase-3 and GFP (p150^{glued}) in cells overexpressing G59S or G71R p150^{glued} was markedly increased compared with control cells (Figure 2E, F). We found that siRNA knockdown against caspase-3 blocked the increase of cell death caused by the overexpression of the mutant p150^{glued} (Figure 2G, H). Next, we wanted to rule out the possibility that extrinsically induced apoptosis via caspase-8 cleavage was causing some or all of the cell death seen in these experiments. Therefore, to exclude this possibility, we examined whether siRNA knockdown of caspase-8 inhibited the apoptosis induced by overexpression of mutant p150^{glued}. Knockdown of caspase-8 did not inhibit apoptosis induced by overexpression of G59S p150^{glued} (Figure S2), suggesting that extrinsically induced apoptosis is not the cause of the cell death seen in these cells.

Aggregate formation caused by the G59S mutant led to cell death. Both aggregate formation and cell death are inhibited by overexpression of Hsp70, a molecular chaperone. These findings suggest that mutant p150^{glued} aggregates play an important role in the mechanism of cell death in HMN7B [11]. We conclude that mutant p150^{glued} aggregates cause apoptosis via activation of the intrinsic apoptotic pathway.

Cells with cytoplasmic aggregates have more mitochondria with reduced mitochondrial membrane potentials

Levy et al. showed that mutant p150^{glued} aggregates are usually associated with mitochondria [11]. Therefore, we hypothesized that an accumulation of damaged mitochondria may cause apoptosis. Live-cell imaging analysis in cells overexpressing WT or mutant p150^{glued} detected elongated tubular mitochondria in control cells, while cells overexpressing mutant p150^{glued} mainly showed fragmented mitochondria in the vicinity of the nuclei (Figure 3A). Overexpression of G59S or G71R p150^{glued} also increased the expression levels of Tom20, a mitochondrial outer membrane protein that is commonly used for assessing mitochondria numbers (Figure 4B, C) [14–16].

To determine the health status of the accumulated mitochondria, we next analyzed cells stained with MitoTracker-Red CMXRos by FACS analysis. Only intact mitochondria with preserved respiration activities and membrane potentials absorb this dye. For an accurate assessment, we only analyzed cells that expressed a high GFP intensity, determined using a flow cytometer. Intriguingly, we detected a marked increase in the number of cells with decreased uptake of MitoTracker-Red CMXRos in cells overexpressing G59S or G71R p150^{glued} compared with the control cells (Figure 3D, E). Also, overexpression of WT p150^{glued} decreased mitochondrial membrane potentials, which might be associated with insufficient mitochondria dynamics [11]. Based on the collected results, we conclude that mutated p150^{glued} causes the accumulation of damaged mitochondria, which is followed by activation of the intrinsic apoptotic pathway.

p150^{glued} knockdown does not affect mitochondrial membrane potentials and activates apoptotic pathway via caspase-8 cleavage

Next, we tested whether or not WT p150^{glued} siRNA knockdown affects mitochondrial functions in a manner similar to mutant p150^{glued} overexpression. As shown in Figure 4A–D, total levels of Tom20 and mitochondria complex I were not changed and the levels of damaged mitochondria without MitoTracker-Red CMX-Ros intake were not significantly increased by p150^{glued} knockdown (Figure 4E, F). Next, we examined caspase-8 activation because of its association with the extrinsic apoptotic pathway. As shown in Figure 5A–H, the levels of total caspase-8 and caspase-3 were decreased with p150^{glued} knockdown, whereas the levels of their cleaved forms of caspase-8 and PARP were increased. This suggests that p150^{glued} knockdown activated caspase-8, leading to caspase-3 activation. Accordingly, treatment with a caspase-8 inhibitor suppressed caspase-3 activation (Figure 5I, J), and caspase-8 siRNA knockdown also decreased apoptotic cell death (Figure 5K, L). Taken together, these data show that the loss-of-function of endogenous p150^{glued} significantly activates caspase-8, inducing apoptosis.

Cells with mutant p150^{glued} overexpression and wild-type endogenous p150^{glued} knockdown showed more apoptosis

Finally, to address the pathogenesis of the p150^{glued}-associated disorders more precisely, we performed mutant p150^{glued} overexpression experiments with or without siRNA knockdown against endogenous p150^{glued}. As shown in Figure 6, siRNA knockdown of endogenous p150^{glued} along with overexpression of either the G59S or G71R mutant form caused many more cells to display early apoptotic changes (GFP-positive and Annexin V-positive)

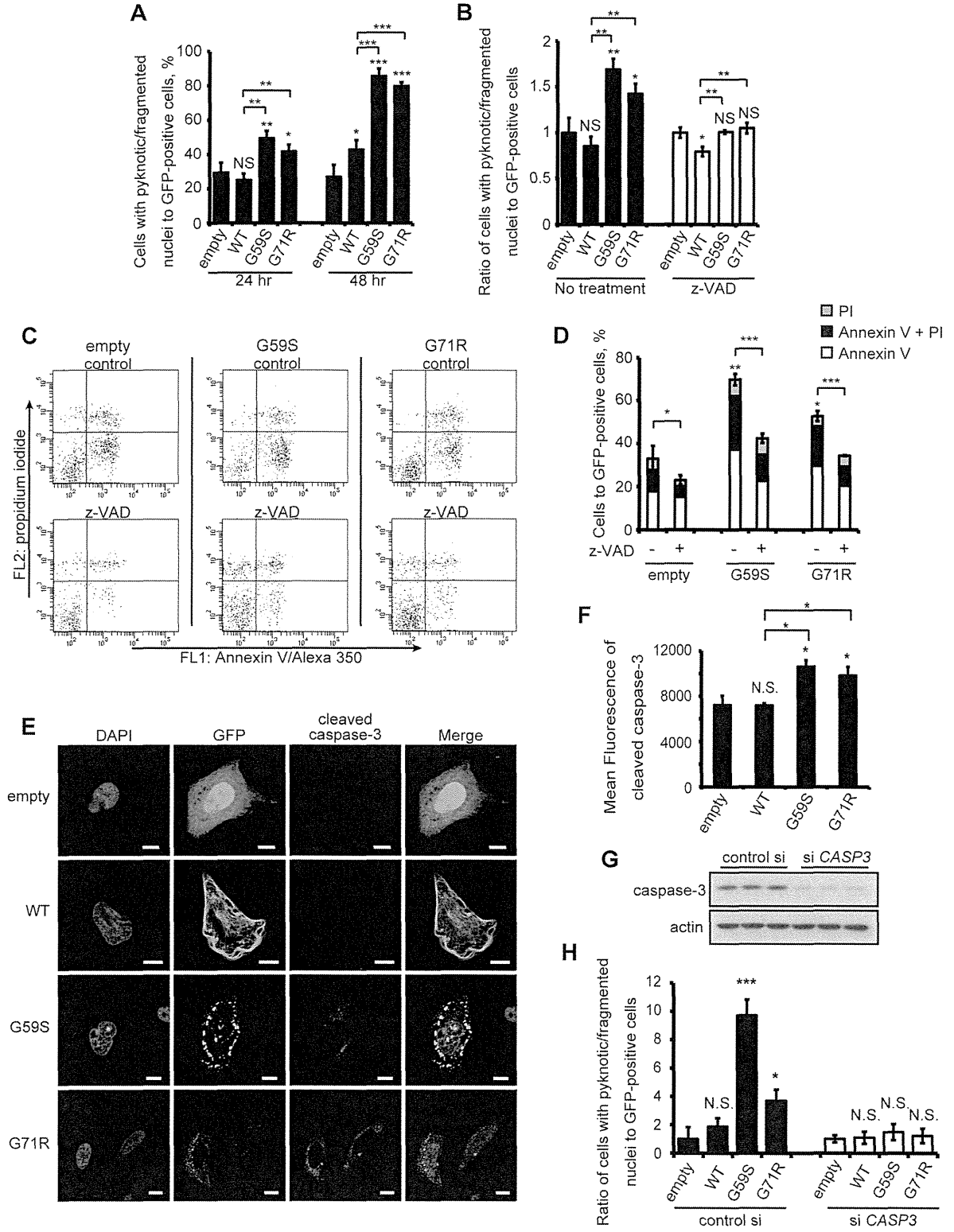

Figure 2. Mutant p150^{glued} proteins activate intrinsic apoptotic pathways. (A) HeLa cells transfected with GFP-empty, GFP-tagged wild-type or mutant (G59S or G71R) p150^{glued} were fixed and stained with DAPI after 24 and 48 h. GFP-positive cells were counted from three independent experiments. The percentage of GFP-positive cells with nuclear abnormalities is shown. (B) Ratio of transfected HeLa cells with nuclear abnormalities

after treatment with or without z-VAD (100 μM) for 24 hours. Values are relative to the GFP-empty value, which is set at 1. (C, D) Transfected SH-SY5Y cells after treatment with or without z-VAD (100 μM) for 48 h were stained with Annexin V and PI, and GFP-positive cells were analyzed by flow cytometry. (E) HeLa cells transfected with GFP-tagged wild-type or mutant p150^{glued} were fixed and stained with an antibody against cleaved caspase-3. Bars, 10 μm. (F) Twenty-four hours after transfection, SH-SY5Y cells were fixed and stained with a cleaved caspase-3 antibody. GFP-positive cells were analyzed by flow cytometry and the mean fluorescent intensity was calculated. (G) HeLa cells were transfected with control scrambled siRNA or caspase-3 siRNA for 72 h and immunoblotting analysis was performed to monitor the knockdown efficiency of the caspase-3 siRNA. (H) Twenty-four hours after transfection with control siRNA or caspase-3 siRNA, HeLa cells were transfected with GFP-empty, GFP-tagged wild-type or mutant p150^{glued}. Forty-eight hours after transfection, cells were fixed and stained with DAPI, and ratios of GFP-positive cells with nuclear abnormalities were analyzed. Values are relative to the GFP-empty value, which is set at 1. The error bar indicates each standard deviation. Statistics are from three independent experiments: N.S., not significant; *, $p<0.05$; **, $p<0.01$; ***, $p<0.001$.
doi:10.1371/journal.pone.0094645.g002

compared with the cells overexpressing a p150^{glued} mutant and a control siRNA. Therefore, we concluded that both excess levels of mutant p150^{glued} and decreased levels of endogenous p150^{glued} contribute to the pathogenesis of p150^{glued}-associated disorders via the activation of apoptosis.

Discussion

In this study, we sought to determine the pathogenesis of p150^{glued}-associated diseases caused by p150^{glued} mutations. Overexpression of mutant p150^{glued} in HeLa and SH-SY5Y cells induced p150^{glued}-positive aggregate formation, accumulation of damaged mitochondria, and activation of the intrinsic apoptotic pathway. Endogenous p150^{glued} knockdown in the same cell lines also activated a caspase-8-dependent apoptotic pathway without apparent mitochondrial abnormalities. Importantly, cell death induced by p150^{glued} knockdown was markedly enhanced by simultaneous overexpression of mutant p150^{glued}, suggesting the disease pathogenesis may be associated with both p150^{glued} gain-of-toxic-function and loss-of-function.

All of the HMN7B and PS associated mutations are located within the CAP-Gly microtubule domain [8], and various reports have suggested that mutant p150^{glued} proteins have the tendency to lose their affinity to microtubules [4,8–10]. Our studies support these reports as we observed decreased colocalization of mutant p150^{glued} with microtubules as well as increased intracytoplasmic aggregates in our immunocytochemistry experiments. However, the *in vivo* binding activity changes of mutant p150^{glued} remain unclear. Therefore, further studies should be performed to determine precisely how mutant p150^{glued} proteins are detoured from their original distribution pattern and how they form aggregates.

The dynein complex plays various critical roles in mitochondrial function (such as retrograde transport and fission/fusion) [17–21]. In this study, we could detect mitochondrial abnormalities (loss of membrane potential and morphological abnormalities) only in cells that expressed mutant forms of p150^{glued}. A report by Varadi et al. found that disruption of dynein function by either p50 overexpression or microinjection of anti-dynein intermediate chain antibodies led to mitochondrial morphology and distribution changes [22]. Our data, however, showed that p150^{glued} siRNA knockdown did not induce mitochondrial abnormalities. Only mutant p150^{glued} overexpression led to these abnormalities, implying that each dynein subunit might have a specific association with mitochondrial function.

Abnormal protein accumulation has been implicated in the pathogenesis of various neurodegenerative diseases [23]. In this study, we revealed that mutant p150^{glued} (G59S, G71R) overexpression induced aggregate formation and caspase activation associated with mitochondrial abnormalities. This supports the findings by Levy et al. who reported that aggregate formation by the G59S mutant leads to cell death, and that both aggregate formation and the induced cell death were inhibited by overexpression of Hsp70, a molecular chaperone [11]. Likewise, other studies have shown that overexpression of a p150^{glued} plasmid with a truncated C-terminal as well as knockdown of endogenous p150^{glued} in rat hippocampal neurons induces caspase-3-positive cell death, which is consistent with our p150^{glued} knockdown results [24,25].

According to studies with *in vivo* models, neither expression of a mutant nor the ΔCAP-Gly domain of p150^{glued} affects axonal transport, but WT p150^{glued} is needed for initiation of retrograde transport at synaptic termini in Drosophila motor neurons and mouse dorsal root ganglion neurons [3,4]. Knock-in and transgenic mice that are heterozygous for the G59S p150^{glued} mutation exhibit late-onset slowly progressive muscle weakness, motor neuron death, and vesicle accumulation [5–7]. This is in contrast to heterozygous p150^{glued} knockout mice, which did not display a neurodegenerative phenotype. Taken together, this evidence suggests that the pathogenesis of p150^{glued}-associated diseases might be caused mainly by a gain-of-function effect [6,26].

Neurons of the hypoglossal nucleus and ventral horn in HMN7B and the substantia nigra and locus coeruleus in PS are substantially affected [1,2]. Although this means that neuronal cell lines are the most appropriate for studying the mechanisms that underlie the pathology of p150^{glued}-associated diseases, various studies have been performed using non-neuronal cell lines. For example, the CAP-Gly domain of p150^{glued} was needed for proper Golgi morphology in HeLa cells [10] and to activate cell division in Drosophila S2 cells [27]. G59S overexpression induced mitochondria-containing p150^{glued} aggregates and insufficient recovery of Golgi distribution following nocodazole treatment in COS7 cells. Overexpression of this mutant also increased cell death induction in MN1 mouse embryonic motor neuron cells [11]; however, this overexpression did not promote apoptosis induction by caspase-3 cleavage in COS7 cells or in rat primary motor neurons [28]. Although our data are from non-polarized and non-neuronal HeLa cells and thus might not reflect the precise physiological state of neurodegenerative disease, we believe that these results give us at least partial insight into the mechanisms underlying p150^{glued}-associated diseases. Further assessment with more appropriate cell lines, like neurons differentiated from induced pluripotent stem cells from the disease patients should be performed in the future.

Materials and Methods

Cell culture and transfection

HeLa and SH-SY5Y cells were maintained as previously described [29]. Cells were transfected using Lipofectamine 2000 (Invitrogen, Carlsbad, CA, USA) according to the manufacturer's protocols. For pharmacological studies, z-VAD-FMK (Calbiochem, San Diego, CA, USA, 219007), caspase-8 inhibitor II (Millipore, Billerica, MA, USA, 218759), and DMSO (Sigma, St.

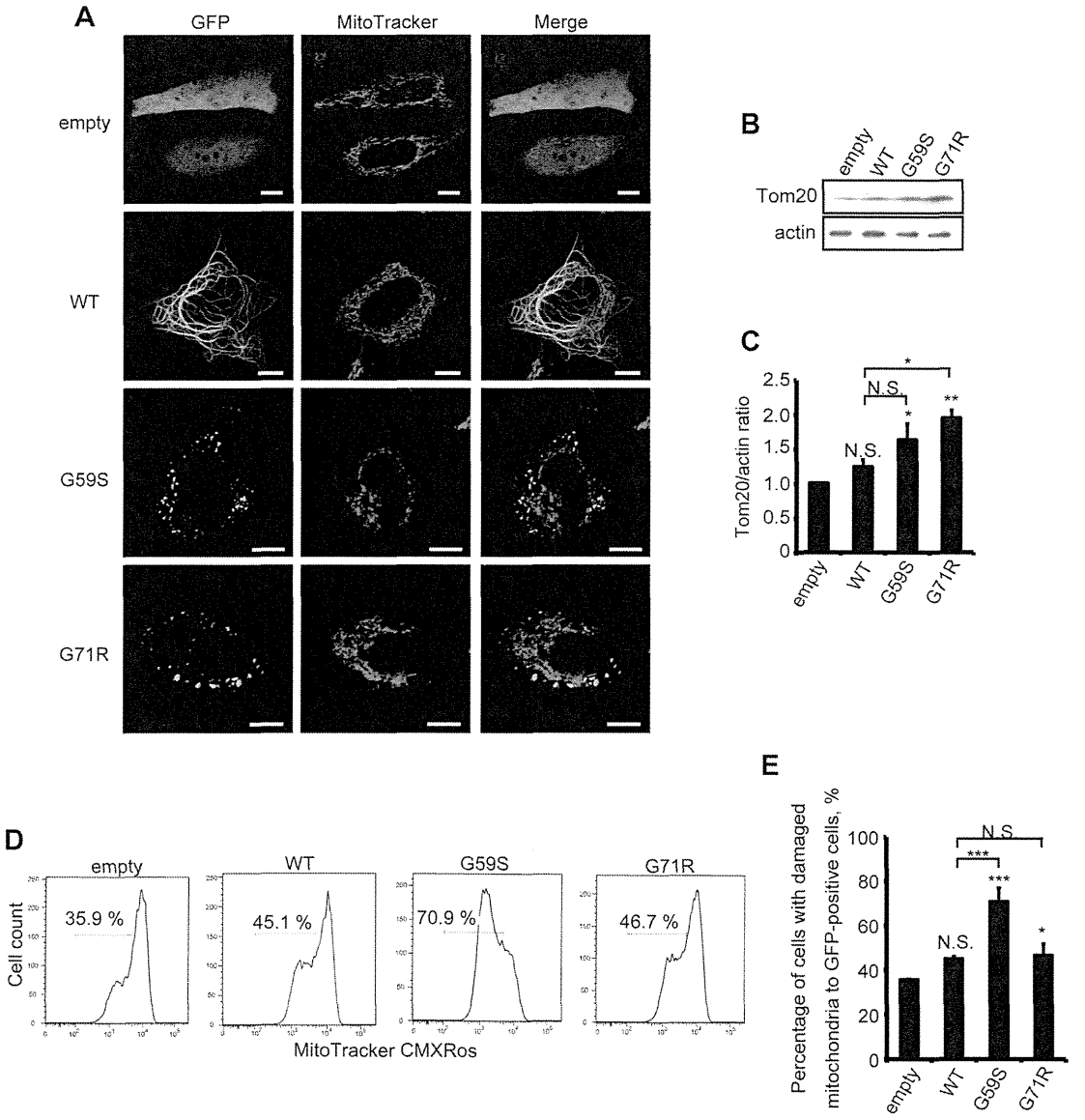

Figure 3. Abnormal mitochondria accumulate in cells overexpressing mutant p150^{glued}. (A) HeLa cells transfected with GFP-empty vector, GFP-tagged wild-type or mutant (G59S or G71R) p150^{glued} were incubated with MitoTracker Deep Red (100 nM) for 15 min and analyzed using confocal microscopy. Insets show higher magnification of the boxed areas. Bars, 10 μm. (B, C) Twenty-four hours after transfection, GFP-positive HeLa cells were sorted using flow cytometry and analyzed by immunoblotting with antibodies against TOM20 and actin (B). Densitometry analysis of TOM20 levels relative to actin was performed in three independent experiments (C). (D, E) Twenty-four hours after transfection, HeLa cells were incubated with Mitotracker-Red CMXRos (25 nM) for 15 min, and intracellular fluorescence intensity was measured by flow cytometry. The histograms of MitoTracker-Red CMXRos fluorescence in GFP-positive cells (D) and the percentages of GFP-positive cells with reduced mitochondrial potentials (E) are shown. The error bar indicates each standard deviation. Statistics are from three independent experiments: *, $p<0.05$; **, $p<0.01$; ***, $p<0.001$.

doi:10.1371/journal.pone.0094645.g003

Louis, MO, USA, D2650) were added at the indicated times and concentrations.

Plasmids

The wild-type *DCTN1* coding region was PCR-amplified from a cDNA plasmid kindly provided by Dr. Farrer MJ (University of British Columbia) using the following primers (Sigma): 5′-TCAAGGGAATTCAATGGCACAGAGCAAGAGGCAC-3′ and 5′-TCAAGGGATATCAGGGAGATGAGGCGACTGT-GAA-3′. The resulting fragment was inserted into the pFLAG-CMV5a vector (Sigma) using *Eco*RV and *Eco*RI. The plasmid was cut with *Eco*RI and *Kpn*I, and the insert was subcloned into pAcGFP-N3 (Clontech, Mountain View, CA, USA). Mutagenesis to create the six mutated p150^{glued} plasmids was performed using the Quikchange Lightning site-directed mutagenesis kit (Stratagene, La Jolla, CA, USA). The pCIneo-TDP43-FLAG plasmid